Dynamics of a hysteretic relay oscillator with periodic forcing

Tamás Kalmár-Nagy, Pankaj Wahi, Abhishek Halder

January 28, 2009

Abstract

The dynamics of a hysteretic relay oscillator with simple harmonic forcing is studied in this paper. Even though there are no bounded solutions in the absence of forcing, periodic excitation gives rise to more complex responses including periodic, quasiperiodic and chaotic behavior. A Poincaré map is introduced to facilitate mathematical analysis. Families of period-one solutions are determined as fixed points of the Poincaré map. These represent coexisting subharmonic responses. Conditions on the amplitude and frequency of the forcing for the existence of periodic solutions have been obtained. Linear stability analysis reveals that these solutions can be classified as centers or saddles. The presence of higher periodic, quasiperiodic motions together with homoclinic and heteroclinic tangles imply the existence of chaotic solutions.

1 Introduction

Over the past decades, relay systems with hysteresis attracted increasing attention. This class of nonlinear systems have found applications in a wide range of engineering problems including voltage regulators, DC motors, and servomechanisms [1, 2, 3, 4, 5, 6, 7]. Relays, in general, have two output branches and the output of a relay jumps discontinuously whenever the input exceeds a certain critical value as shown in Fig. 1. For an ideal relay, there is a single critical value for which the output is discontinuous while for a relay with hysteresis, there are two such critical input values as shown in Fig. 1.

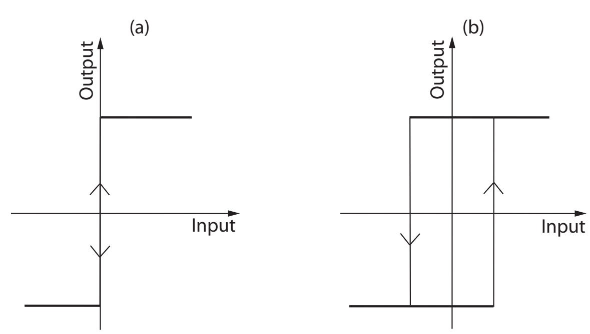

Figure 1: Input-output characteristics of (a) an ideal relay and (b) a relay with hysteresis.

Andronov [2] and Åström [7] studied the existence and stability of period-one solutions (i.e., solutions having exactly two relay switchings per period). Gonçalves *et al.* [8, 9] presented a global analysis of relay systems using Lyapunov functions. Johansson *et al.* and di Bernardo *et al.* extensively studied different aspects of feedback systems with ideal relays (see [10, 11, 12] and references therein). Periodic solutions in a relay system with square-wave excitation was considered by Varigonda and Georgiou [3], while Fleishman [13] focused on periodic response under sinusoidal forcing. A related class of nonlinear systems involve relay operators with delays in the input. Barton *et al.* [14], Fridman *et al.* [15], and Norbury and Wilson [16] considered first order delayed relay systems while Bayer and Heiden [17], Sieber [18], Barton *et al.* [19] and Colombo *et al.* [20] studied second order systems. These studies include periodic solutions, their bifurcations as well as chaotic solutions in these systems with or without forcing.

Hysteretic relay operators are also used in modeling complex hysteresis in materials where they are commonly known as the elementary Preisach operators [21, 22]. However, studies on the response of hysteretic systems modeled using relay operators [23, 24] almost always neglect the dynamics of the relay operators.

Relay systems belong to the general class of piecewise smooth dynamical systems. Other systems belonging to this class include systems with play or backlash [25], systems with friction [26, 27, 28, 29, 30], systems with impacts [26, 27, 28, 30, 31, 32, 33, 34, 35], and other hybrid systems [36, 37, 38, 39]. Leine and van Campen [26] provide an overview and examples of bifurcation phenomena in such non-smooth dynamical systems. In particular, the relay system considered in this study is a piecewise linear system which is similar to the much studied repeated impact of a ball with a sinusoidally vibrating table [31, 40, 41, 42, 43, 44, 45] and its Hamiltonian analog studied in relevance to particle physics [46, 47, 48]. Further, the equation studied in this paper can also be taken as a simple model for automotive suspension with magneto-rheological (MR) damper [49] under periodic forcing.

In this paper, we study the dynamics of a hysteretic relay operator under periodic excitation. It is shown that in this system, a rich variety of dynamic responses ranging from periodic to chaotic solutions exist. We obtain conditions on the parameters, i.e., amplitude and frequency of the forcing for which bounded solutions can exist. To facilitate the analysis, we introduce a 2D Poincaré map. Fixed points of the Poincaré map correspond to periodic solutions of the system. There are two families of period-one solutions corresponding to two families of fixed points of the Poincaré map. On the Poincaré plane, one family of fixed points corresponds to centers while the other corresponds to saddles. There are invariant curves around the centers on the Poincaré plane which correspond to quasiperiodic solutions. The presence of homoclinic tangles has been shown numerically. This indicates the existence of chaotic solutions. As the parameters are varied, the centers and the saddles merge in a saddle-center bifurcation [50, 51]. For these parameter values, there is a single family of non-hyperbolic fixed points corresponding to a single family of period-one solutions with no other bounded solutions.

2 Mathematical model of the relay oscillator

The equation studied in this work is

$$\ddot{x}(t) + F[x(t)] = A\cos(\omega t + \phi)\,,\ \ A \geq 0\,,\, \omega > 0,\, \phi \in (-\pi, \pi]\,. \tag{1}$$

Where A, ω, and ϕ are the amplitude, frequency, and phase of the forcing, respectively. The hysteretic relay operator $F[x(t)]$ (shown in Fig. 2) is defined as

$$F[x(t)] = \begin{cases} -1, & x(t) \leq 0 \\ e, & 0 < x(t) < 1 \\ 1, & x(t) \geq 1 \end{cases} \tag{2}$$

where e is -1 or 1 depending on the initial conditions and the time history of the solution, i.e., whether the solution enters the hysteretic region $0 < x(t) < 1$ from the left or right. When $F[x(t)] = \mp 1$, the evolution of the

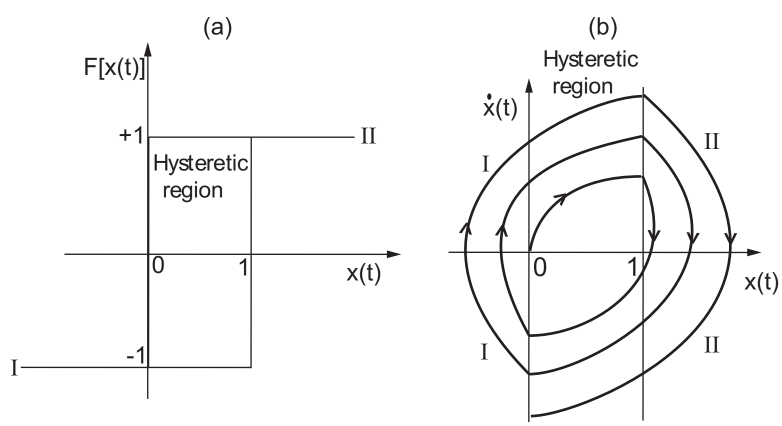

Figure 2: (a) The relay operator with hysteresis. (b) Phase portrait of (1) for A=0. Initial conditions are $x(0) = 0$ and $\dot{x}(0) = 0$.

dynamical system is described by

$$(I) \quad \ddot{x}_I(t) - 1 = A\cos(\omega t + \phi_I), \tag{3}$$
$$(II) \quad \ddot{x}_{II}(t) + 1 = A\cos(\omega t + \phi_{II})\ , \tag{4}$$

where the subscripts are used to differentiate between the two subsystems. The complete description of the system also requires initial conditions. Without loss of generality, these initial conditions can be specified as

$$F[x(0)] = -1\,, \quad x_I\,(0) = 0, \quad \dot{x}_I\,(0) = v_I. \tag{5}$$

Figure 2(b) shows the phase portrait in $x(t)$ and $\dot{x}(t)$ for the free response of the system (i.e., $A = 0$, see section 4). The dynamics switches between the subsystems when the solution trajectories intersect $x_I(t) = 1$ from the left, i.e., $\dot{x}_I(t) \geq 0$ or $x_{II}(t) = 0$ from the right, i.e., $\dot{x}_{II}(t) \leq 0$.

To make the analysis simpler, time is reset when transition occurs between subsystems. To account for this artificial time-shift, the phase of the forcing is 'updated' at the switchings. Therefore, the evolution of the dynamics is completely specified by

$$\ddot{x}_I(t) - 1 = A\cos(\omega t + \phi_I)\,,\ x_I(0) = 0, \dot{x}_I(0) = v_I,\, t \in [0, t_I] \tag{6}$$

$$\ddot{x}_{II}(t) + 1 = A\cos(\omega t + \phi_{II})\,,\ \ x_{II}(0) = 1, \dot{x}_{II}(0) = v_{II},\, t \in [0, t_{II}]. \tag{7}$$

Here t_I and t_{II} are the switching times defined implicitly by $x_I(t_I) = 1$ and $x_{II}(t_{II}) = 0$, respectively.

3 The phase space and solutions

Figure 3(a) depicts the evolution of solution trajectories in $x(t)$, $\dot{x}(t)$ and $F[x(t)]$. Time t is introduced as another

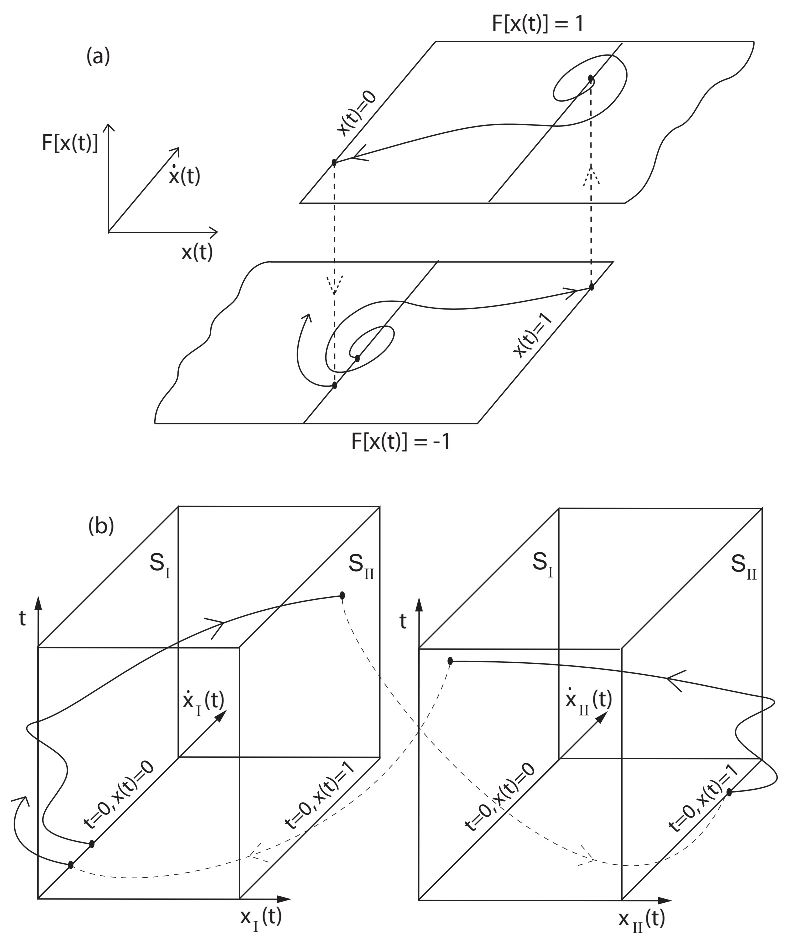

Figure 3: (a) Phase space of (1) in $x(t)$, $\dot{x}(t)$ and $F[x(t)]$. (b) Extended phase space $(x_I(t), \dot{x}_I(t), t) \bigcup (x_{II}(t), \dot{x}_{II}(t), t)$

state variable resulting in an extended phase space [25, 31]. Clearly $x_I(t) \in X_I = (-\infty, -1]$ and $x_{II}(t) \in X_{II} = [0, \infty)$. Also, $\dot{x}_I(t), \dot{x}_{II}(t) \in \mathbb{R}$ and $t \in \mathbb{R}^+$. The extended phase space is therefore $X_I \times \mathbb{R} \times \mathbb{R}^+ \bigcup X_{II} \times \mathbb{R} \times \mathbb{R}^+$. This space is a proper subset of $\mathbb{R}^3 \times \{-1, 1\}$, where the discrete set $\{-1, 1\}$ is simply the range of $F[x(t)]$.

It is again emphasized in Fig. 3 that the system consists of two distinct subsystems, viz. subsystem I and subsystem II. The dynamics of subsystem I switches to that of subsystem II when the solution trajectories intersect the surface $S_{II} = \{(\dot{x}(t), t) \,|\, x(t) = 1,\, \dot{x}(t) \geq 0\}$ and from subsystem II to subsystem I when they intersect the plane $S_I = \{(\dot{x}(t), t) \,|\, x(t) = 0,\, \dot{x}(t) \leq 0\})$ as demonstrated in Fig. 3(b).

Having described the structure of the phase space, we now turn our attention to the solutions. The solution of subsystem I can be written in closed form as

$$x_I(t) = \frac{1}{2}t^2 + \left(v_I - \frac{A}{\omega}\sin(\phi_I)\right)t + \frac{A}{\omega^2}\cos(\phi_I) - \frac{A}{\omega^2}\cos(\omega t + \phi_I), \tag{8}$$

$$\dot{x}_I(t) = t + v_I - \frac{A}{\omega}\sin(\phi_I) + \frac{A}{\omega}\sin(\omega t + \phi_I)\,. \tag{9}$$

Similarly, the solution of subsystem II is

$$x_{II}(t) = 1 - \frac{1}{2}t^2 + \left(v_{II} - \frac{A}{\omega}\sin(\phi_{II})\right)t + \frac{A}{\omega^2}\cos(\phi_{II}) - \frac{A}{\omega^2}\cos(\omega t + \phi_{II}), \tag{10}$$

$$\dot{x}_{II}(t) = -t + v_{II} - \frac{A}{\omega}\sin(\phi_{II}) + \frac{A}{\omega}\sin(\omega t + \phi_{II})\,. \tag{11}$$

Note that the transformation $(v_I, \phi_I) \to (-v_{II}, \phi_{II} + \pi)$ in Eqs. (8) and (9) is equivalent to

$$(x_I(t),\, \dot{x}_I(t)) \to (1 - x_{II}(t), -\dot{x}_{II}(t))\,, \tag{12}$$

and the substitution $(v_{II}, \phi_{II}) \to (-v_I, \phi_I + \pi)$ in Eqs. (10) and (11) leads to

$$(x_{II}(t),\, \dot{x}_{II}(t)) \to (1 - x_I(t), -\dot{x}_I(t))\,. \tag{13}$$

Therefore a solution of one subsystem with an initial velocity v and initial phase of the forcing ϕ also represents solution trajectories of the other subsystem with the corresponding initial velocity $-v$ and initial phase $\phi + \pi$. As a consequence, solutions appear in pairs, i.e. if $(x(t), \dot{x}(t))$ is a solution of Eq. (1), then so is $(1 - x(t), -\dot{x}(t))$. This motivates the introduction of the 'shift map'

$$\Psi\begin{pmatrix} v \\ \phi \end{pmatrix} = \begin{pmatrix} -1 & 0 \\ 0 & 1 \end{pmatrix}\begin{pmatrix} v \\ \phi \end{pmatrix} + \begin{pmatrix} 0 \\ \pi \end{pmatrix}. \tag{14}$$

which maps solutions of subsystem I into those of subsystem II. This map will be utilized in Section 6 during the construction of the Poincaré map.

Having established some properties of the solutions, we proceed with our analysis of the model. First, the free response of the model is discussed.

4 Free response

In this section, we show that in the absence of forcing, i.e., $A = 0$, all solutions of the system are unbounded. The system is now given by

$$\ddot{x}(t) + F[x(t)] = 0\,. \tag{15}$$

The solution of the subsystems I and II for this case becomes

$$x_I(t) = \frac{1}{2}\,t^2 + v_I\,t \tag{16}$$

$$\dot{x}_I(t) = t + v_I\,, \tag{17}$$

and

$$x_{II}(t) = 1 - \frac{1}{2}\,t^2 + v_{II}\,t \tag{18}$$

$$\dot{x}_{II}(t) = -t + v_{II}\,. \tag{19}$$

When $x_I(t_I) = 1$, the system switches from subsystem I to subsystem II. The equation determining the switching time t_I is therefore

$$\frac{1}{2}\,t_I^2 + v_I\,t_I - 1 = 0\,, \tag{20}$$

which can be solved in closed form to give (for $t_I > 0$)

$$t_I = -v_I + \sqrt{v_I^2 + 2}\,. \tag{21}$$

Substituting t_I in Eq. (17), we get the velocity at the switching as

$$\dot{x}_I(t_I) = -v_I + \sqrt{v_I^2 + 2} + v_I = \sqrt{v_I^2 + 2}\,.$$

The initial velocity for the subsystem II is $\dot{x}_{II}(0) = v_{II} = \dot{x}_I(t_I)$. Substituting $v_{II} = \sqrt{v_I^2 + 2}$ in Eq. (18), the solution $x_{II}(t)$ is given by

$$x_{II}(t) = 1 - \frac{1}{2}\,t^2 + \sqrt{v_I^2 + 2}\;t\,. \tag{22}$$

The switch from subsystem II to subsystem I occurs when $x_{II}(t_{II}) = 0$. This yields

$$1 - \frac{1}{2}\,t_{II}^2 + \sqrt{v_I^2 + 2}\;t_{II}\; = 0\,. \tag{23}$$

The above equation can again be solved in closed form (for $t_{II} > 0$) to give

$$t_{II} = \sqrt{v_I^2 + 2} + \sqrt{v_I^2 + 4}\,. \tag{24}$$

Substituting t_{II} from Eq. (24) into Eq. (19), we get

$$v_{II}(t_{II}) = -\sqrt{v_I^2 + 4}\,. \tag{25}$$

which is also the next initial velocity for subsystem I, i.e. $\dot{x}_I(0) = v_I = v_{II}(t_{II})$. From Eq. (25), we note that the absolute velocity of the system at switchings is monotonically increasing without bound. The phase portrait depicted in Fig. 2(b) actually corresponds to the free response with $x(0) = 0$ and $\dot{x}(0) = v_I = 0$. The unbounded growth of the solution at switchings, can easily be seen in the figure.

Next we consider the case $A > 0$. For a detailed analysis of the forced response, it is convenient to introduce a Poincaré map [25, 31] and study this discrete map instead of the continuous evolution of the system. In the next Section, we compute the switching times that will be needed for obtaining the Poincaré map.

5 Switching times

In order to find the switching time t_I at which transition takes place between subsystems I and II, the switching criterion $x_I(t_I) = 1$ is substituted into Eq. (8) resulting in

$$\frac{1}{2}t_I^2 + \left(v_I - \frac{A}{\omega}\sin(\phi_I)\right)t_I + \frac{A}{\omega^2}\cos(\phi_I) - \frac{A}{\omega^2}\cos(\omega t_I + \phi_I) - 1 = 0\,. \tag{26}$$

The switching time t_I is the first positive root of Eq. (26) and is a function of v_I and ϕ_I for fixed A and ω. Due to the transcendental nature of the equation numerical solution is required (details of the numerical algorithm is provided in the Appendix A. It will be shown that when $A \leqslant 1$, the algorithm works irrespective of the value of ω). The function $t_I\,(v_I, \phi_I)$ can have discontinuities corresponding to grazing bifurcations [52, 53] depending on the parameters A and ω (this is discussed in detail in Appendix B). The velocity at the transition (from Eq. (9)) is

$$\dot{x}_I(t_I) = t_I + v_I - \frac{A}{\omega}\sin(\phi_I) + \frac{A}{\omega}\sin(\omega t_I + \phi_I)\,. \tag{27}$$

The phase of the forcing at the transition is simply

$$\phi_I + \omega\, t_I \bmod 2\,\pi\,. \tag{28}$$

Similarly, to find the time t_{II} of the transition from subsystem II to subsystem I, the switching criterion $x_{II}(t_{II}) = 0$ is substituted into equation Eq. (10) to yield

$$-\frac{1}{2}t_{II}^2 + \left(v_{II} - \frac{A}{\omega}\sin(\phi_{II})\right)t_{II} + \frac{A}{\omega^2}\cos(\phi_{II}) - \frac{A}{\omega^2}\cos(\omega t_{II} + \phi_{II})\; + 1 = 0\,. \tag{29}$$

The switching time t_{II} is the smallest positive root of this equation. The velocity at the transition is (from Eq. (11))

$$\dot{x}_{II}(t_{II}) = -t_{II} + v_{II} - \frac{A}{\omega}\sin(\phi_{II}) + \frac{A}{\omega}\sin(\omega t_{II} + \phi_{II}) \tag{30}$$

and the phase is $\phi_{II} + \omega\, t_{II} \bmod 2\,\pi$. From here on, the modulo 2π notation for the phase variable will not be explicitly written out.

Next, we outline the procedure for obtaining the discrete Poincaré map.

6 Poincaré map

With the knowledge of the switching times, we are now in the position to construct a map to effectively study the behavior of solutions of Eq. (1). First, consider the mapping $(\dot{x}_I(0) = v_I, \phi_I) \to (\dot{x}_I(t_I), \phi_I + \omega\, t_I)$ of the initial velocity and phase to the velocity and phase at the time of the transition from subsystem I to subsystem II. Recall that the initial and final positions are uniquely specified by $x_I(0) = 0$ and $x_I(t_I) = 1$. As already mentioned in Section 4, the final velocity and phase for the solution of subsystem I at the transition (Eqs. (27) and (28)) will serve as initial velocity and phase for the solution of subsystem II, i.e.

$$v_{II} = \dot{x}_I(t_I) = t_I + v_I - \frac{A}{\omega}\sin(\phi_I) + \frac{A}{\omega}\sin(\phi_{II}), \tag{31}$$

$$\phi_{II} = \phi_I + \omega\, t_I. \tag{32}$$

Similarly, the final values of velocity and phase of the solution of subsystem II will provide the initial conditions for the solution of subsystem I as

$$v_I = \dot{x}_{II}(t_{II}) = -t_{II} + v_{II} - \frac{A}{\omega}\sin(\phi_{II}) + \frac{A}{\omega}\sin(\phi_I), \tag{33}$$

$$\phi_I = \phi_{II} + \omega\, t_{II}. \tag{34}$$

Rearranging Eqs. (31) and (33) yields

$$v_{II} - \frac{A}{\omega}\sin(\phi_{II}) = t_I + v_I - \frac{A}{\omega}\sin(\phi_I), \tag{35}$$

$$v_I - \frac{A}{\omega}\sin(\phi_I) = -t_{II} + v_{II} - \frac{A}{\omega}\sin(\phi_{II})\,. \tag{36}$$

The form of these expressions motivates the introduction of a new variable $z = v - \frac{A}{\omega}\sin(\phi)$[1]. Equations (35) and (36) can now be rewritten as

$$z_{II} = t_I + z_I\,, \tag{37}$$

$$z_I = -t_{II} + z_{II}, \tag{38}$$

where $z_I = v_I - \frac{A}{\omega}\sin(\phi_I)$ and $z_{II} = v_{II} - \frac{A}{\omega}\sin(\phi_{II})$. We can now relate initial values of the variables z, ϕ to their values at the switchings by the two maps Π_I, Π_{II} as

$$\begin{pmatrix} z_{II} \\ \phi_{II} \end{pmatrix} = \Pi_I \begin{pmatrix} z_I \\ \phi_I \end{pmatrix} = \begin{pmatrix} z_I + t_I \\ \phi_I + \omega t_I \end{pmatrix}. \tag{39}$$

$$\begin{pmatrix} z_I \\ \phi_I \end{pmatrix} = \Pi_{II} \begin{pmatrix} z_{II} \\ \phi_{II} \end{pmatrix} = \begin{pmatrix} z_{II} - t_{II} \\ \phi_{II} + \omega t_{II} \end{pmatrix}. \tag{40}$$

Note that Eq. (40) can also be written as

$$\Pi_{II} \begin{pmatrix} z_{II} \\ \phi_{II} \end{pmatrix} = \begin{pmatrix} z_{II} - t_{II} \\ \phi_{II} + \omega t_{II} \end{pmatrix} = \Psi \circ \Pi_I \circ \Psi \begin{pmatrix} z_{II} \\ \phi_{II} \end{pmatrix}, \tag{41}$$

where Ψ is the shift map introduced in Eq. (14). To specify the range and domain of these maps, we introduce the Poincaré surfaces $\Sigma_I = \{(z_I, \phi_I) | x(t) = 0\}$ and $\Sigma_{II} = \{(z_{II}, \phi_{II}) | x(t) = 1\}$. Clearly, Π_I and Π_{II} are maps from Σ_I onto Σ_{II} and from Σ_{II} onto Σ_I, respectively. The Poincaré map (a.k.a. return map) Π is now defined

[1] z is the velocity component induced by the hysteretic force field $F[x(t)]$. It can also be viewed as the relative velocity between the solution trajectories of Eq. (1) with $F[x(t)]$ as defined in Eq. (2) with $F[x(t)] \equiv 0$.

as the map of the plane Σ_I onto itself after a pair of switchings. The map Π is therefore obtained by composing the two maps Π_{II} and Π_I as

$$\Pi\begin{pmatrix} z_I \\ \phi_I \end{pmatrix} = \Pi_{II}\circ\Pi_I\begin{pmatrix} z_I \\ \phi_I \end{pmatrix} = \Psi\circ\Pi_I\circ\Psi\circ\Pi_I\begin{pmatrix} z_I \\ \phi_I \end{pmatrix}, \tag{42}$$

where the last equality comes from Eq. (41). The final expression for the Poincaré map in Eq. (42) again emphasizes the symmetry in the problem. Substituting Eqs. (39) and (40) for Π_I and Π_{II} into Eq. (42) results in

$$\Pi\begin{pmatrix} z_I \\ \phi_I \end{pmatrix} = \begin{pmatrix} z_I + t_I(z_I,\phi_I) - t_{II}(z_I,\phi_I) \\ \phi_I + \omega t_I(z_I,\phi_I) + \omega t_{II}(z_I,\phi_I) \end{pmatrix}. \tag{43}$$

Equation (43) defines the Poincaré map Π to be used in the subsequent analysis. The implicit dependence of the switching times t_I and t_{II} on (z_I,ϕ_I) is also emphasized. With the new variables z_I and z_{II} introduced in Eqs. (26) and (29), the switching times t_I and t_{II} are determined as the first positive roots of

$$\frac{1}{2}t_I^2 + z_I t_I + \frac{A}{\omega^2}\cos(\phi_I) - \frac{A}{\omega^2}\cos(\omega t_I + \phi_I) - 1 = 0\,, \tag{44}$$

$$-\frac{1}{2}t_{II}^2 + z_{II} t_{II} + \frac{A}{\omega^2}\cos(\phi_{II}) - \frac{A}{\omega^2}\cos(\omega t_{II} + \phi_{II}) + 1 = 0\,, \tag{45}$$

respectively. Substituting for z_{II} and ϕ_{II} from Eqs. (37) and (32) into Eq. (45) results in

$$-\frac{1}{2}t_{II}^2 + (z_I + t_I)t_{II} + \frac{A}{\omega^2}\cos(\phi_I + \omega t_I) - \frac{A}{\omega^2}\cos(\phi_I + \omega t_I + \omega t_{II}) + 1 = 0\,. \tag{46}$$

Equations (44) and (46) now define the implicit dependence of t_I and t_{II} on (z_I,ϕ_I). As mentioned previously, the switching times are not necessarily continuous functions of the parameters and depending on the parameters A and ω, the switching times t_I and t_{II} can in general have discontinuities corresponding to grazing bifurcations [52, 53] as z_I and ϕ_I are varied. This will result a discontinuous Poincaré map leading to further complexity of the system. However, in this work, we only consider parameter values A and ω for which the switching times and consequently the Poincaré map are continuous (Appendix B discusses conditions for which this parametric continuity holds).

With the introduction of the Poincaré map we have reduced the study of the original hybrid system (1) to that of the discrete map $\Pi : \Sigma_I \to \Sigma_{II}$. After having obtained the Poincaré map, we now wish to calculate its inverse, to be utilized later for discussing global dynamics of the system.

7 Inverse Poincaré map

The Poincaré map was defined as the return map from the surface Σ_I to itself after a pair of switchings and is described by

$$\Pi\begin{pmatrix} z_I \\ \phi_I \end{pmatrix} = \Pi_{II}\circ\Pi_I\begin{pmatrix} z_I \\ \phi_I \end{pmatrix},$$

where Π_I is the map from the surface Σ_I to Σ_{II} while Π_{II} is the map from the surface Σ_{II} to Σ_I. The inverse Poincaré map is given by

$$\Pi^{-1}\begin{pmatrix} z_I \\ \phi_I \end{pmatrix} = \Pi_I^{-1}\circ\Pi_{II}^{-1}\begin{pmatrix} z_I \\ \phi_I \end{pmatrix}. \tag{47}$$

Hence, the map Π is invertible iff the individual maps Π_I and Π_{II} are invertible. We will assume that the individual maps Π_I and Π_{II} are invertible and hence, the maps Π_I^{-1} and Π_{II}^{-1} are uniquely defined. The domain and range of the map Π_I^{-1} are the switching surfaces Σ_{II} and Σ_I, respectively, while the domain and the range of the map Π_{II}^{-1} are the switching surfaces Σ_I and Σ_{II}, respectively. The inverse map will be used in Section 9 to compute backward iterations.

The inverse Poincaré map Π^{-1} is given by the transformation $t \to t_I + t_{II} - t$. Further, the above transformation implies the transformations $(z_I,\phi_I) \to (-z_I,-\phi_I)$ and $(z_{II},\phi_{II}) \to (-z_{II},-\phi_{II})$ for the variables z and ϕ on the switching surfaces. Thus, using these two transformations, one can compute the individual inverse maps Π_{II}^{-1} and Π_I^{-1} and following (47), take their composition to obtain the inverse Poincaré map. However, a more straightforward derivation results if one resorts to the equivalent transformation $t \to t_I + t_{II} - t$. In view of this transformation, from (43), it follows that (dropping the modulo 2π notation for the phase variable as before)

$$\Pi^{-1}\begin{pmatrix} z_I \\ \phi_I \end{pmatrix} = \Pi_I^{-1} \circ \Pi_{II}^{-1}\begin{pmatrix} z_I \\ \phi_I \end{pmatrix} = \begin{pmatrix} z_I - t_I + t_{II} \\ \phi_I - \omega\, t_I - \omega\, t_{II} \end{pmatrix}, \tag{48}$$

where t_I and t_{II} are the corresponding switching times to be determined.

To determine switching times t_I and t_{II} for this case, we first recall that the domain of Π_{II}^{-1} is Σ_I. Accordingly, the initial conditions for the subsystem II for the inverse map are $x_{II}(0) = 0$, $\dot{x}_{II}(0) = -z_I - \dfrac{A}{\omega}\sin(\phi_I)$. With these initial conditions, the solution for the subsystem II is

$$x_{II}(t) = -\frac{1}{2}\,t^2 - z_I\,t + \frac{A}{\omega^2}\cos(-\phi_I) - \frac{A}{\omega^2}\cos(\omega\,t - \phi_I)\,,$$

$$\dot{x}_{II}(t) = -t - z_I + \frac{A}{\omega}\sin(\omega\,t - \phi_I)\,.$$

Hence, the switching time t_{II} from the subsystem II to the subsystem I using the switching criterion $x_{II}(t) = 1$ is the root of the equation

$$-\frac{1}{2}\,t_{II}^2 - z_I\,t_{II} + \frac{A}{\omega^2}\cos(-\phi_I) - \frac{A}{\omega^2}\cos(\omega\,t_{II} - \phi_I) - 1 \;=\; 0$$

which can be rewritten as

$$\frac{1}{2}\,t_{II}^2 + z_I\,t_{II} - \frac{A}{\omega^2}\cos(-\phi_I) + \frac{A}{\omega^2}\cos(\omega\,t_{II} - \phi_I) + 1 \;=\; 0\,. \tag{49}$$

At the instant of switching from subsystem II to subsystem I, we have $\dot{x}_{II} \leq 0$. The first root of Eq. (49) is associated with $\dot{x}_{II} \geq 0$ and therefore, the switching time t_{II} is the first root of Eq. (49) if $\dot{x}_{II}(t_{II}) = 0$, otherwise it is the second root of Eq. (49).

Similarly the initial conditions for the subsystem I for the inverse map are $x_I(0) = 1$, $\dot{x}_I(0) = -z_{II} - \dfrac{A}{\omega}\sin(\phi_{II})$. With these initial conditions, the solution for the subsystem I is

$$x_I(t) = 1 + \frac{1}{2}\,t^2 - z_{II}\,t + \frac{A}{\omega^2}\cos(-\phi_{II}) - \frac{A}{\omega^2}\cos(\omega\,t - \phi_{II})\,,$$

$$\dot{x}_I(t) = t - z_{II} + \frac{A}{\omega}\sin(\omega\,t - \phi_{II})\,.$$

Using the above solution along with the switching criterion $x_I(t) = 0$ results in

$$1 + \frac{1}{2}\,t_I^2 - z_{II}\,t_I + \frac{A}{\omega^2}\cos(-\phi_{II}) - \frac{A}{\omega^2}\cos(\omega\,t_I - \phi_{II}) \;=\; 0 \tag{50}$$

which yields the switching time t_I from the subsystem I to subsystem II as its second root.

The switching times t_I and t_{II} thus obtained as the second roots of Eqs. (49) and (50) respectively, need to be substituted in (48) to complete the derivation of the inverse Poincaré map. In the following section, we proceed to study the periodic solutions of the system.

8 Periodic solutions

We first locate period-one solutions of Eq. (1), i.e., solutions which involve a single pair of switchings between Σ_I and Σ_{II}. Equivalently, we are looking for the fixed points of the Poincaré map Π.

8.1 Period-one solutions

Fixed points of the Poincaré map are given by

$$\begin{pmatrix} z_I^* \\ \phi_I^* \end{pmatrix} = \Pi\begin{pmatrix} z_I^* \\ \phi_I^* \end{pmatrix}.$$

Accordingly, Eq. (43) yields the conditions

$$z_I^* = z_I^* + t_I - t_{II}\,, \tag{51}$$

$$\phi_I^* = \phi_I^* + \omega\, t_I + \omega\, t_{II}. \tag{52}$$

Equation (51) gives

$$t_I = t_{II}\,, \tag{53}$$

which after substitution into Eq. (52) results in

$$t_I = t_{II} = \frac{n\,\pi}{\omega}, \tag{54}$$

since $t > 0$, $n \in \mathbb{Z}^+$. Having obtained the switching times t_I and t_{II} for a fixed point of the Poincaré map, we still need to determine the values of z_I^* and ϕ_I^*. Using Eqs. (44), (46) and (54), we obtain

$$\frac{n^2\pi^2}{2\,\omega^2} + z_I^*\frac{n\pi}{\omega} - 1 + \frac{A\cos(\phi_I^*)}{\omega^2}(1-(-1)^n)\ = 0 \tag{55}$$

and

$$\frac{n^2\pi^2}{2\,\omega^2} + z_I^*\frac{n\pi}{\omega} + 1 + \frac{A\cos(\phi_I^*)}{\omega^2}\,((-1)^n - 1)\ = 0\,. \tag{56}$$

Subtracting Eq. (55) from Eq. (56) yields

$$2 + 2\frac{A\cos(\phi_I^*)}{\omega^2}\,((-1)^n - 1)\ = 0\,. \tag{57}$$

Equation (57) can only be solved for odd n to yield

$$\cos(\phi_I^*) = \frac{\omega^2}{2\,A}. \tag{58}$$

Recall that $A > 0$. Since $|\cos(\phi_I^*)| \leq 1$, the condition for existence of a period-one solution is given by

$$\omega^2 \leq 2A\,. \tag{59}$$

From Eq. (58), the initial phase ϕ_I^* corresponding to the period-one solution is obtained as

$$\phi_I^* = \pm\arccos\left(\frac{\omega^2}{2A}\right)\,. \tag{60}$$

Adding Eqs. (55) and (56), we have

$$\frac{n^2\pi^2}{\omega^2} + 2\,z_I^*\frac{n\pi}{\omega} = 0$$

which can be solved for z_I^* to give

$$z_I^* = -\frac{n\,\pi}{2\,\omega}\,, \qquad n = 1, 3, 5, \cdots\,. \tag{61}$$

The countably many values of n in Eq. (61) together with the two values of ϕ_I^* given by Eq. (60) define two families of fixed points of the Poincaré map for a given set of parameters A and ω as

$$(z_I^*, \phi_I^*)_{1,2} = \left(-\frac{n\,\pi}{2\,\omega}, \pm\arccos\left(\frac{\omega^2}{2A}\right)\right),\ \ n = 1, 3, 5, \cdots\,. \tag{62}$$

Each of these fixed points corresponds to a period-one solution of Eq. (1). The $x(t)$-$\dot{x}(t)$ portraits of the system corresponding to $n = 1, 3, 5$ and 7 are shown in Fig. 4. These different period-one motions represent $1 : n$ subharmonic resonances of the system and they coexist for a given set of parameter values. The period-one solutions shown in Fig. 4 corresponding to $(-\pi/2, \pi/3)$, $(-\pi/2, -\pi/3)$, $(-3\pi/2, \pi/3)$ and $(-3\pi/2, -\pi/3)$ are plotted together in Fig. 5 to emphasize their coexistence. The initial conditions for each $x(t)$-$\dot{x}(t)$ portrait has been chosen to be consistent with the fixed points given in Eq. (62), i.e., for $A = 1$, $\omega = 1$ and $n = 1$, the initial conditions corresponding to $z_I = -\pi/2$ and $\phi_I = -\pi/3$ are $x(0) = 0$ and $\dot{x}(0) = -\pi/2 - \sqrt{3}/2$.

Having obtained the conditions for the existence of period-one solutions of the system governed by Eq. (1), or equivalently the fixed points of the Poincaré map Eq. (43), we perform stability analysis of these fixed points in the next section.

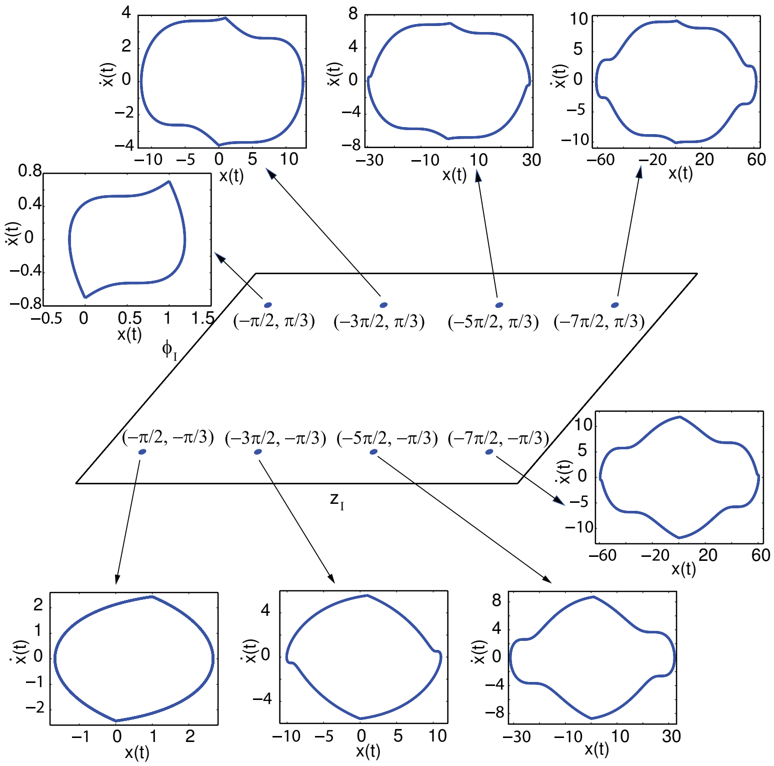

Figure 4: $x(t)$-$\dot{x}(t)$ portraits for $A = 1$ and $\omega = 1$ corresponding to the fixed points of the Poincaré map for $n = 1, 3, 5$ and 7.

8.2 Stability analysis of period-one solutions

For the purpose of stability analysis of the fixed points of the Poincaré map Eq. (43), we calculate the linearized Poincaré map about the fixed points (z_I^*, ϕ_I^*) using a perturbation expansion. The linearized Poincaré map $D\Pi$ of map (43) can be written as

$$D\Pi = \begin{pmatrix} 1 + \frac{\partial t_I}{\partial z_I} - \frac{\partial t_{II}}{\partial z_I} & \frac{\partial t_I}{\partial \phi_I} - \frac{\partial t_{II}}{\partial \phi_I} \\ \omega \left(\frac{\partial t_I}{\partial z_I} + \frac{\partial t_{II}}{\partial z_I} \right) & 1 + \omega \left(\frac{\partial t_I}{\partial \phi_I} + \frac{\partial t_{II}}{\partial \phi_I} \right) \end{pmatrix}. \tag{63}$$

The derivatives $\frac{\partial t_I}{\partial z_I}$, $\frac{\partial t_I}{\partial \phi_I}$, $\frac{\partial t_{II}}{\partial z_I}$ and $\frac{\partial t_{II}}{\partial \phi_I}$ are obtained by differentiating Eqs. (44) and (46) w.r.t. the variables z_I and ϕ_I. For example

$$\frac{\partial t_I}{\partial z_I} = -\frac{\omega\, t_I}{\omega\ (z_I + t_I) + A\ \sin(\omega\, t_I + \phi_I)},$$

$$\frac{\partial t_I}{\partial \phi_I} = \frac{A\,(\sin(\phi_I) - \sin(\omega\, t_I + \phi_I))}{\omega\,(\omega\ (z_I + t_I) + A\ \sin(\omega\, t_I + \phi_I))}.$$

The expressions for $\frac{\partial t_{II}}{\partial z_I}$ and $\frac{\partial t_{II}}{\partial \phi_I}$ are a bit lengthier. However, when evaluated at the fixed points, these expressions can be simplified (with the introduction of new variables p, q, r and s) as follows

$$\left.\frac{\partial t_I}{\partial z_I}\right|_{(z_I^*, \phi_I^*)} = \frac{n\,\pi}{A\ \sin(\phi_I^*) - \omega\, z_I^* - n\,\pi} = p \tag{64}$$

and

$$\left.\frac{\partial t_I}{\partial \phi_I}\right|_{(z_I^*, \phi_I^*)} = \frac{2\,A\ \sin(\phi_I^*)}{\omega\,(A\ \sin(\phi_I^*) - \omega\, z_I^* - n\,\pi)} = q. \tag{65}$$

$$\left.\frac{\partial t_{II}}{\partial z_I}\right|_{(z_I^*, \phi_I^*)} = \frac{n\,\pi\,(\omega\, z_I^* - 3\,A\ \sin(\phi_I^*))}{(A \sin(\phi_I^*) + \omega Z_I^*)\,(A \sin(\phi_I^*) - \omega\, z_I^* - n\pi)} = r \tag{66}$$

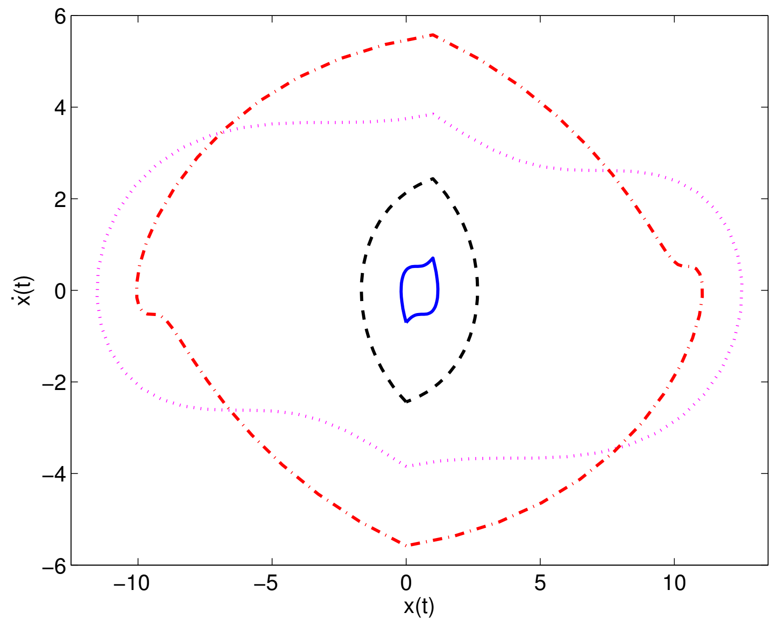

Figure 5: $x(t)$-$\dot{x}(t)$ portraits for $A = 1$ and $\omega = 1$ corresponding to the fixed points $(-\pi/2, \pi/3)$ (solid line), $(-\pi/2, -\pi/3)$ (dashed line), $(-3\pi/2, \pi/3)$ (dotted line) and $(-3\pi/2, -\pi/3)$ (dash-dotted line).

and

$$\left.\frac{\partial t_{II}}{\partial \phi_I}\right|_{(z_I^*, \phi_I^*)} = \frac{2\,A\sin(\phi_I^*)\,(\omega\, z_I^* + \,A\sin(\phi_I^*) + 2\,n\pi\,)}{\omega\,(A\sin(\phi_I^*) + \omega Z_I^*)\,(A\sin(\phi_I^*) - \omega\, z_I^* - n\pi)} = s. \tag{67}$$

Now the linearized Poincaré map ($D\Pi$) governing the evolution of the perturbations around the fixed point (z_I^*, ϕ_I^*) can be represented succinctly as

$$D\Pi = \begin{pmatrix} 1 + p - r & q - s \\ \omega(p + r) & 1 + \omega(q + s) \end{pmatrix}. \tag{68}$$

The eigenvalues of the matrix $D\Pi$ determine the stability of the fixed points of the Poincaré map Eq. (43) or equivalently the period-one solutions of the system Eq. (1). The eigenvalues of $D\Pi$ are given by

$$\lambda_{1,2} = -\frac{\mathrm{tr}\,(D\Pi)}{2} \pm \frac{\sqrt{\mathrm{tr}\,(D\Pi)^2 - 4\,\det(D\Pi)}}{2}, \tag{69}$$

where

$$\mathrm{tr}\,(D\Pi) = 2 + p - r + \omega(q + s)$$

and

$$\det(D\Pi) = 1 + p - r + \omega\,(2ps + 2qr + q + s)\,.$$

Substituting for p, q, r and s from (64)-(67) in the above, it is easy to verify that $\det(D\Pi) = 1$ and

$$\mathrm{tr}\,(D\Pi) = \frac{2\,(2\,A\,\sin(\phi_I^*) + n\,\pi)^2 + 16\,A\,n\,\pi\,\sin(\phi_I^*)}{(2\,A\,\sin(\phi_I^*) - n\,\pi)^2}. \tag{70}$$

Since $\lambda_1\,\lambda_2 = \det(D\Pi) = 1$, there are three possibilities for the eigenvalues:

1. Both λ_1 and λ_2 are real and distinct. In this case, one has a modulus greater than one (eigenvalue outside the unit circle) and the other smaller than one (eigenvalue inside the unit circle). This fixed point is a saddle.

2. λ_1 and λ_2 are complex conjugate with $|\lambda_1| = |\lambda_2| = 1$ (eigenvalues on the unit circle). The fixed point is a center.

3. Either $\lambda_1 = \lambda_2 = 1$ or $\lambda_1 = \lambda_2 = -1$. The fixed point is a non-hyperbolic fixed point and nonlinear analysis is required to determine the behavior of the fixed point.

From Eq. (69), we note that the eigenvalues $\lambda_{1,2}$ are real and distinct if $\mathrm{tr}\,(D\Pi) > 2$, and they are complex conjugate if $\mathrm{tr}\,(D\Pi) < 2$. Substituting $\phi_I^* = \arccos\left(\dfrac{\omega^2}{2\,A}\right)$ in Eq. (70) gives

$$\mathrm{tr}\,(D\Pi) = \frac{2\left(4\,A^2 - \omega^4 + n^2\pi^2 + 6\,n\,\pi\,\sqrt{4\,A^2-\omega^4}\right)}{4\,A^2 - \omega^4 + n^2\pi^2 - 2\,n\,\pi\,\sqrt{4\,A^2-\omega^4}}\,.$$

Clearly $\mathrm{tr}\,(D\Pi) > 2$ for $\omega < \sqrt{2\,A}$ and hence, the eigenvalues are real and distinct. Therefore, the family of fixed points corresponding to $\phi_I^* = \arccos\left(\dfrac{\omega^2}{2A}\right)$ are saddles. Similarly, a substitution of $\phi_I^* = -\arccos\left(\dfrac{\omega^2}{2\,A}\right)$ results in

$$\mathrm{tr}\,(D\Pi) = \frac{2\left(4\,A^2 - \omega^4 + n^2\pi^2 - 6\,n\,\pi\,\sqrt{4\,A^2-\omega^4}\right)}{4\,A^2 - \omega^4 + n^2\pi^2 + 2\,n\,\pi\,\sqrt{4\,A^2-\omega^4}} < 2$$

for $\omega < \sqrt{2\,A}$. Hence, the family of fixed points corresponding to $\phi_I^* = -\arccos\left(\dfrac{\omega^2}{2A}\right)$ are centers. These two branches of period-one solutions are shown in Fig. 6.

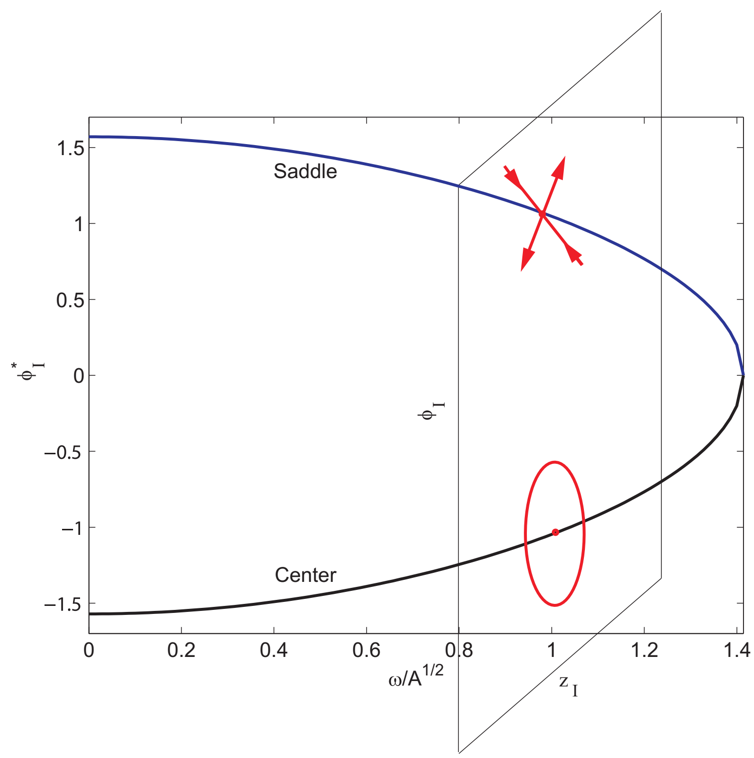

Figure 6: The two branches of fixed points of the Poincaré map Eq. (43).

In the limiting case of $\omega^2 = 2\,A$, the saddle and the center merge in a saddle-center bifurcation [50, 51] leaving a single family of fixed points

$$(z_I^*, \phi_I^*) = \left(\frac{-n\,\pi}{2\,\sqrt{2\,A}}, 0\right) \qquad n = 1, 3, 5, \cdots.$$

At these points both the eigenvalues are equal to 1. Therefore, this represents a family of non-hyperbolic fixed points.

8.3 Higher-period solutions

In this section, we illustrate the procedure for a period-2 solution only. The procedure for higher periodic solutions is similar. A period-2 solution of Eq. (1) is a fixed point of the map Π^2. The sequence of switching times for Eq. (1) are denoted as $t_I, t_{II}, t_{III}, t_{IV}, \cdots$. Denoting the fixed point of the map Π^2 as (z_I^{**}, ϕ_I^{**}), from Eq. (43) we have

$$\begin{pmatrix} z_I^{**} \\ \phi_I^{**} \end{pmatrix} = \Pi \circ \Pi \begin{pmatrix} z_I^{**} \\ \phi_I^{**} \end{pmatrix} = \begin{pmatrix} z_I^{**} + t_I - t_{II} + t_{III} - t_{IV} \\ \phi_I^{**} + \omega\,(t_I + t_{II} + t_{III} + t_{IV}) \end{pmatrix}$$

From the above, we get two equations, viz.

$$t_I - t_{II} + t_{III} - t_{IV} = 0 \tag{71}$$

and

$$\omega\,(t_I + t_{II} + t_{III} + t_{IV}) = 2\,n\,\pi \tag{72}$$

for some integer n. We require four more equations in order to be able to solve for the six unknowns z_I^{**}, ϕ_I^{**}, t_I, t_{II}, t_{III} and t_{IV}. These equations come from the four switching criteria, $x_I(t_I) = 1$, $x_{II}(t_{II}) = 0$, $x_I(t_{III}) = 1$ and $x_{II}(t_{IV}) = 0$. Substituting for the appropriate initial conditions in each case, these equations are given by

$$\frac{1}{2}t_I^2 + z_I^{**} t_I + \frac{A}{\omega^2}\cos(\phi_I^{**}) - \frac{A}{\omega^2}\cos(\phi_I^{**} + \omega t_I) - 1 = 0\,, \tag{73}$$

$$-\frac{1}{2}t_{II}^2 + (z_I^{**} + t_I)\,t_{II} + \frac{A}{\omega^2}\cos(\phi_I^{**} + \omega t_I) - \frac{A}{\omega^2}\cos(\phi_I^{**} + \omega t_I + \omega t_{II}) + 1 = 0\,, \tag{74}$$

$$\frac{1}{2}t_{III}^2 + (z_I^{**} + t_I - t_{II})\,t_{III} + \frac{A}{\omega^2}\cos(\phi_I^{**} + \omega t_I + \omega t_{II}) - \frac{A}{\omega^2}\cos(\phi_I^{**} + \omega t_I + \omega t_{II} + \omega t_{III}) - 1 = 0\,, \tag{75}$$

$$\begin{aligned} -\frac{1}{2}t_{IV}^2 + (z_I^{**} + t_I - t_{II} + t_{III})\,t_{IV} + \frac{A}{\omega^2}\cos(\phi_I^{**} + \omega t_I + \omega t_{II} + \omega t_{III}) - \\ \frac{A}{\omega^2}\cos(\phi_I^{**} + \omega t_I + \omega t_{II} + \omega t_{III} + \omega t_{IV}) + 1 = 0\,. \end{aligned} \tag{76}$$

Equations (71)-(76) need to be solved for the six unknowns z_I^{**}, ϕ_I^{**}, t_I, t_{II}, t_{III} and t_{IV} numerically. In our simulations, we found no period-2 solutions. However, we found four period-3 solutions which are shown in Fig. 7. These period-3 solutions appear in pairs as noted previously. Solutions a and b form a center-type pair, while solutions c and d form a saddle-type pair. This is concluded from the numerical evaluation of the eigenvalues of the linearized Poincaré map, i.e., the Floquet multipliers associated with the numerically obtained period-three solution pair. These solution pairs have the symmetry defined by Eqs. (12) and (13) as $(x_b(t), \dot{x}_b(t)) = (1 - x_a(t), \dot{x}_a(t))$ and $(x_a(t), \dot{x}_a(t)) = (1 - x_b(t), \dot{x}_b(t))$ where the subscripts a and b are used to refer to the solutions a and b in Fig. 7. We also found other higher odd period solution pairs and some even period solution pairs. The phase portrait corresponding to the period-8 and period-14 solutions obtained for $A = 1$ and $\omega = 1/2$ are shown in Figs. 8 and 9, respectively.

8.4 Quasiperiodic solutions

It has been observed numerically that there are invariant curves surrounding the center which correspond to quasiperiodic solutions of Eq. (1). The trajectory of Eq. (1) in the $x(t)$-$\dot{x}(t)$ plane corresponding to one of this quasiperiodic solutions for the first few cycles is shown in Fig. 10. A 3D plot corresponding to the quasiperiodic solution shown in Fig. 10 (using a delayed value of the state variable $x(t)$ as a new variable [54]) is depicted in Fig. 11. The delayed state is used here only for the purpose of illustration. Figure 11 shows that the quasiperiodic solutions lie on a torus. Also plotted in the figure is the period-three solution a (from Fig. 7 again) to emphasize the coexistence of the quasiperiodic and the period-three solutions.

The winding numbers of these quasiperiodic solutions [45] measure the average rotation induced by the Poincaré map on the Poincaré plane. These prove useful in the classification of the different quasiperiodic solutions, viz., the ones associated with the invariant curves around the center-type period-one solutions and those around the center-type higher periodic solution pairs. To illustrate this, the winding numbers of the quasiperiodic solutions as a function of the distance from the first period-one solution along the $\phi_I = \phi_I^*$ line are plotted in Fig. 12. The plateaus in Fig. 12 at $z_I - z_I^* = 0.4$ (0.33) correspond to the period-five (period-three) and associated quasiperiodic solutions around them.

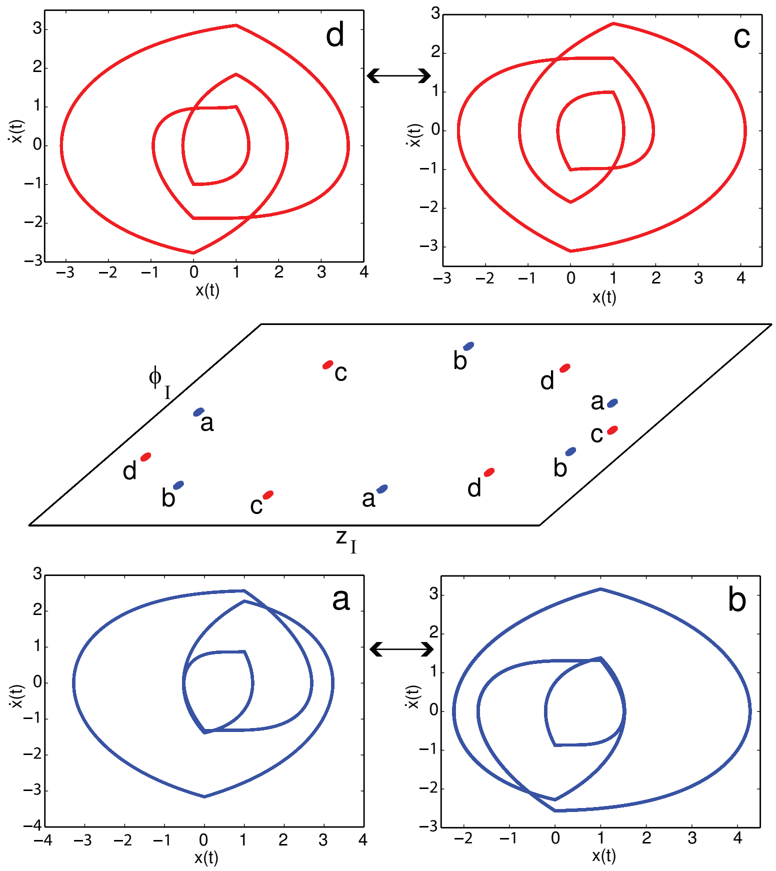

Figure 7: $x(t)$-$\dot{x}(t)$ portraits of the period-three solutions of Eq. (1) for $A = 1$ and $\omega = 1$.

9 Global dynamics

The presence of centers and saddles on the Poincaré plane hints towards possible homoclinic and heteroclinic orbits or tangles. The dynamics of the system in the z-ϕ variables on the Poincaré plane for $A = 1$ and $\omega = 1$ is shown in Fig. 13. Here we have shown the dynamics around the first three centers and saddles. The eigenvector for the first saddle is also plotted in the figure and matches well with the numerically observed directions of the stable and unstable manifolds of the saddle. While it seems that there is a homoclinic orbit around the center, the unstable and the stable manifolds of the saddles intersect transversally giving rise to chaotic tangles. A zoomed view of the boxed portion of Fig. 13 (bottom) is shown in Fig. 13 (top). Here, we notice the presence of isolated invariant curves close to the apparent homoclinic orbit. These isolated curves correspond to quasiperiodic solutions around the center type period-three solution pair. Also shown are the approximate heteroclinic connections between the saddle type period-three solution pair. The presence of several higher period solution pairs hints toward the existence of a Smale horseshoe [31, 55] related to the transverse intersection of the stable and unstable manifolds of the saddle. In Fig. 14, we have plotted the result of forward and backward iterations of 250×250 points in a small neighborhood of the saddle. To compute the backward iterations, the inverse Poincaré map presented in Section 7 is used. The transverse intersection of the stable and the unstable manifolds of the saddle is clearly visible in Fig. 14. This numerical evidence shows the existence of a Smale horseshoe which imply the existence of an infinite number of higher periodic and bounded aperiodic solutions.

At the saddle-center bifurcation point, we have a single family of non-hyperbolic fixed points on the Poincaré plane.

10 Conclusions

Dynamics of a system with a hysteretic relay operator with simple harmonic forcing is studied in this paper. A Poincaré map has been introduced to facilitate the analysis. Conditions on the amplitude and frequency of the

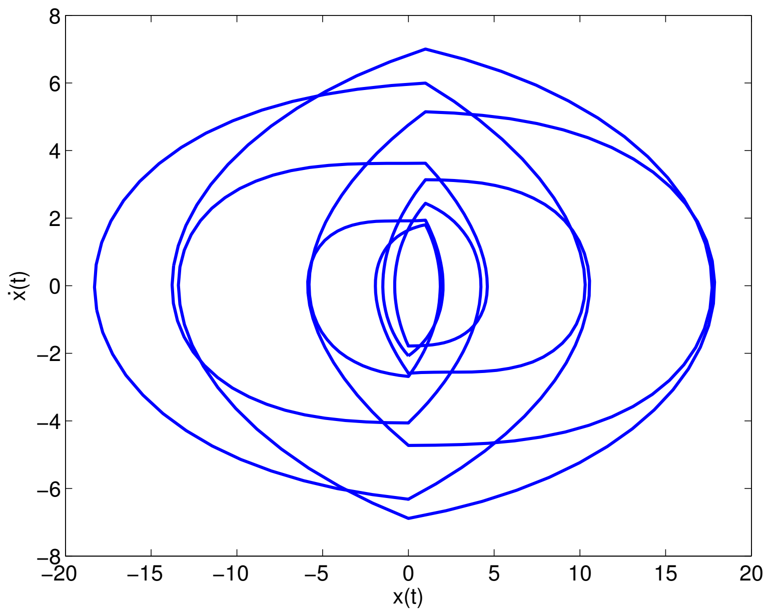

Figure 8: $x(t)$-$\dot{x}(t)$ portrait of the period-8 solution of Eq. (1) for $A = 1$ and $\omega = 1/2$. Initial conditions: $z_I = -0.1328$ and $\phi_I = -1.3325$

forcing for the existence of periodic solutions have been obtained. There are two families of period-one solutions determined as the fixed points of the Poincaré map. On the Poincaré plane, one family of the fixed points is a center and the other one is a saddle. Higher-period solutions have been obtained numerically. Invariant curves surrounding the center on the Poincaré plane have been obtained which correspond to quasiperiodic solutions. Homoclinic and heteroclinic tangles have been observed numerically implying the presence of chaotic solutions.

References

[1] Tsypkin, Ya. Z., 1984, *Relay Control Systems*, Cambridge University Press, Cambridge, UK.

[2] Andronov, A. A., Vitt, A. A., and Khaikin, S. E., 1966, *Theory of oscillators*, Dover publications, New York, USA.

[3] Varigonda, S., and Georgiou, T. T., 2001, "Dynamics of relay relaxation oscillators", *IEEE Transactions on Automatic Control,* **46**(1), pp. 65-77.

[4] Zhusubaliev, Zh. T., and Titov, V. S., 2001, "Chaotic oscillations in the relay system with hysteresis", *Automation and Remote Control*, **62**(1), pp. 55-66.

[5] Postnikov, N. S., 1997, "Dynamic chaos in relay systems with hysteresis", *Computational Mathematics and Modeling*, **8**(1), pp. 62-72.

[6] Zhusubaliev, Zh. T., and Soukhoterin, E. A., 2002, "Oscillations in a relay control system with hysteresis and time dead zone", *Mathematics and Computers in Simulation*, **58**(4), pp. 329-350.

[7] Åström, K. J., 1995, "Oscillations in systems with relay feedback", *Adaptive Control, Filtering, and Signal Processing*, (K. J. Åström, G. C. Goodwin, and P. R. Kumar, Ed.s), Springer-Verlag, New York, USA, pp. 1-25.

[8] Gonçalves, J. M., Megretski, A., and Dahleh, M. A., 2001, "Global stability of relay feedback system", *IEEE Transactions on Automatic Control*, **46**(4), pp. 550-562.

[9] Gonçalves, J. M., Megretski, A., and Dahleh, M. A., 2003, "Global analysis of piecewise linear systems using impact maps and surface Lyapunov functions", *IEEE Transactions on Automatic Control*, **48**(12), pp. 2089-2106.

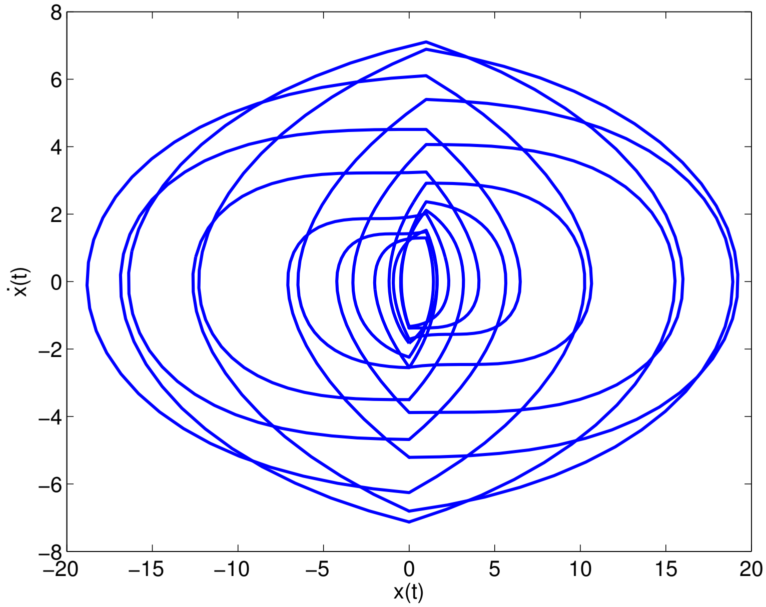

Figure 9: $x(t)$-$\dot{x}(t)$ portrait of the period-14 solution of Eq. (1) for $A = 1$ and $\omega = 1/2$. Initial conditions: $z_I = 0.1067$ and $\phi_I = -1.3203$

[10] Johansson, K. H., Rantzer, A., and Åström, K. J., 1999, "Fast switches in relay feedback systems", *Automatica*, **35**(4), pp. 539-552.

[11] di Bernardo, M., Johansson, K. H., and Vasca, F., 2001. "Self-oscillations and sliding in relay feedback systems: Symmetry and bifurcations", *International Journal of Bifurcation and Chaos*, **11**(4), pp. 1121-1140.

[12] di Bernardo, M., Johansson, K. H., Jönsson, U., and Francesco, V., 2002, "On the robustness of periodic solutions in relay feedback systems", *Proceedings of the Fifteenth IFAC Triennial World Congress*, Barcelona, Spain.

[13] Fleishman, B. A., 1965, "Forced oscillations and convex superposition in piecewise-linear systems", *SIAM Review*, **7**(2), pp. 205-222.

[14] Barton, D. A. W., Krauskopf, B., and Wilson, R. E., 2005, "Explicit periodic solutions in a model of a relay controller with delay and forcing", *Nonlinearity*. **18**(6), pp. 2637-2656.

[15] Fridman, E., Fridman, L., and Shustin, E., 2000, "Steady modes in relay control systems with time delay and periodic disturbances", *ASME Journal of Dynamic Systems, Measurements and Control*, **122**, pp. 732-737.

[16] Norbury, J., and Wilson, R. E., 2000, "Dynamics of constrained differential delay equations", *Journal of Computational and Applied Mathematics*, **125**, pp. 201-215.

[17] Bayer, W., and Heiden, U., 1998, "Oscillation types and bifurcations of a nonlinear second-order differential-difference equation", *Journal of Dynamics and Differential Equations*, **10**(2), pp. 303-326.

[18] Sieber, J., 2006, "Dynamics of delayed relay systems", *Nonlinearity*, **19**, pp. 2489-2527.

[19] Barton, D. A. W., Krauskopf, B., and Wilson, R. E., 2006, "Periodic solutions and their bifurcations in a non-smooth second-order delay differential equation", *Dynamical Systems*. **21**(3), pp. 289-311.

[20] Colombo, A., di Bernardo, M., Hogan, S. J., and Kowalczyk, P., 2006, "Complex dynamics in a hysteretic relay feedback system with delay" to appear in *Journal of Nonlinear Science*.

[21] Mayergoyz, I. D., 2003, *Mathematical Models of Hysteresis and their Applications*, Elsevier, New York, USA.

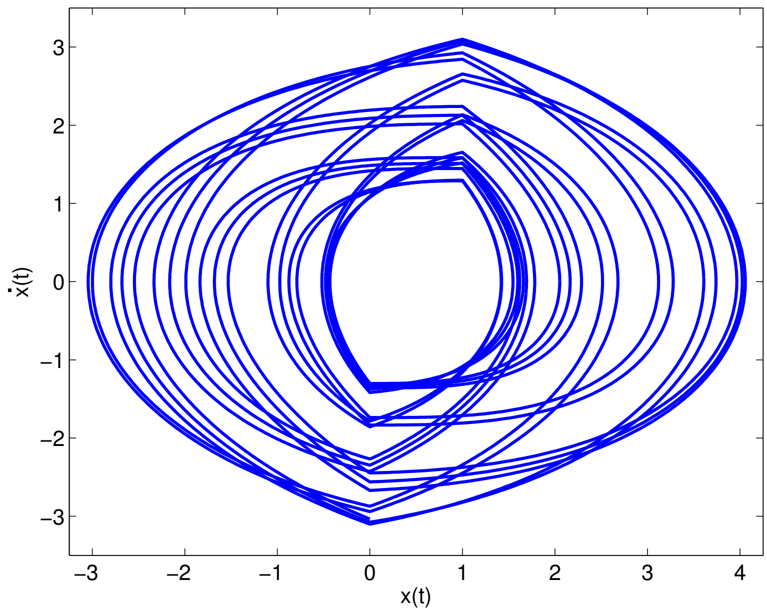

Figure 10: $x(t)$-$\dot{x}(t)$ portrait corresponding to a quasiperiodic solution of Eq. (1) for $A = 1$ and $\omega = 1$. Initial conditions correspond to $z_I = -0.97$ and $\phi_I = -\pi/3$, i.e., $x(0) = 0$ and $\dot{x}(0) = -1.83$.

[22] Krasonoselśkii, M. A., and Pokrovskii, A. V., 1983, *Systems with Hysteresis*, Springer-Verlag, Berlin, Germany.

[23] Spanos, P. D., Kontsos, A., and Cacciola, P., 2006, "Steady-state dynamic response of Preisach hysteretic systems", *ASME Journal of Vibration and Acoustics*, **128**, pp. 244-250.

[24] Krejči, P., 2000, "Forced oscillations in Preisach systems", *Physica B*, **275**, pp. 81-86.

[25] Kleczka, M., Kreuzer, E., and Schiehlen, W., 1992, "Local and Global Stability of a Piecewise Linear Oscillator", *Philosophical Transactions of the Royal Society of London*, **338**, pp. 533-546.

[26] Leine, R. I., and Nijmeijer, H., 2004, *Dynamics and Bifurcations of Non-Smooth Mechanical Systems*, Springer, New York, USA.

[27] Kunze, M., 2000, *Non-smooth Dynamical Systems*, Springer, New York, USA.

[28] Brogliato, B, 1999, *Nonsmooth Mechanics: Models, Dynamics and Control*, Springer, New York, USA.

[29] Oestreich, M., Hinrichs, N., and Popp, K., 1996 "Bifurcation and stability analysis for a non-smooth friction oscillator", *Archives of Applied Mechanics*, **66**(5), pp. 301-314.

[30] Hinrichs, N., Oestreich, M., and Popp, K., 1997 "Dynamics of Oscillators with Impact and Friction", *Chaos, Solitons and Fractals*, **8**(4), pp. 535-558.

[31] Guckenheimer, J., and Holmes, P., 2002, *Nonlinear Oscillations, Dynamical systems, and Bifurcations of Vector Fields*, Springer-Verlag, New York, USA.

[32] Pavlovskaia, E. E., and Wiercigroch, M., 2005, "Two dimensional map for impact oscillator with drift", in *Proceedings of the IUTAM Symposium on Chaotic Dynamics and Control of Systems and Processes in Mechanics*, pp. 305-312.

[33] Ing, J., Pavlovskaia, E. E., and Wiercigroch, M., 2006, "Dynamics of a nearly symmetrical piecewise linear oscillator close to grazing incidence: modelling and experimental verification" *Nonlinear Dynamics*, **46**, pp. 225-238.

[34] Chin, W., Ott, E., Nusse, H. E., and Grebogi, C., 1994, "Grazing bifurcations in impact oscillators", *Physical Review E*, **50**(6), pp. 4427-4444.

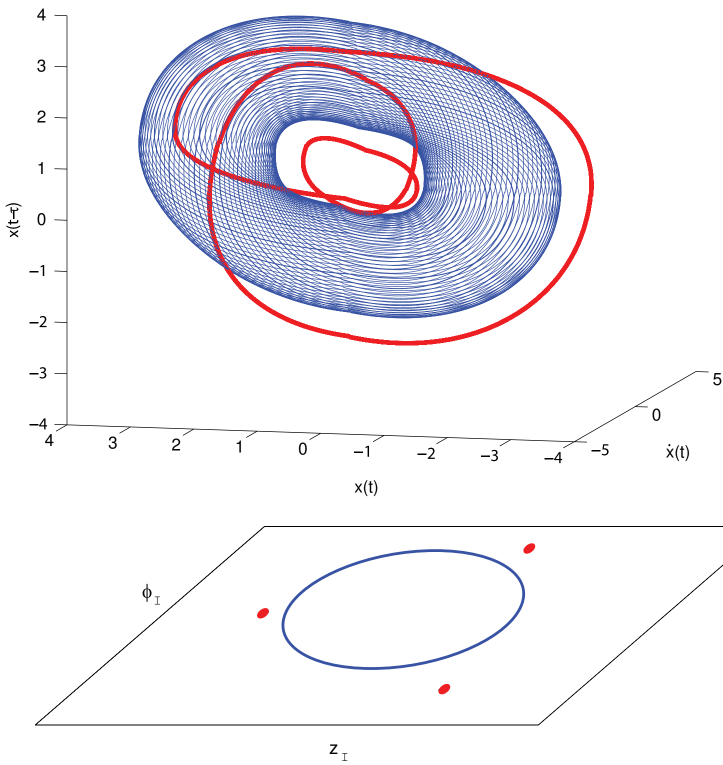

Figure 11: 3D plot in $x(t)$-$\dot{x}(t)$-$x(t-\tau)$ space with $\tau = \pi/2$ corresponding to Fig. 10. The thick curve represents one of the three-period solutions corresponding to Fig. 7

[35] Shaw, S. W., and Holmes, P. J., 1983. "A periodically forced piecewise linear oscillator", *Journal of Sound and Vibration*, **90**(1), pp. 129-155.

[36] Lygeros, J., Johansson, K. H., Simic, S. N., Zhang, J., and Sastry, S., 2003, "Dynamical properties of hybrid automata", *IEEE Transactions on Automatic Control*, **48**, pp. 2-17.

[37] Oishi, M. K., Mitchell, I. M., Bayen, A. M., and Tomlin, C. J., 2006, "Hybrid system verification: application to user-interface design", *to appear in IEEE Transactions on Control Systems Technology*, 2006.

[38] Sanfelice, R. G., Goebel, R., and Teel, A. R., 2006, "A feedback control motivation for generalized solutions to hybrid systems", *Proceedings 9th International Workshop on Hybrid Systems: Computation and Control*, **3927**, pp. 522-536.

[39] Alur, R., Henzinger, T. A., and Sontag, E. D., 1996, *Hybrid Systems III. Verification and Control*, Springer-Verlag, Berlin.

[40] Holmes, P. J., 1982, "The dynamics of repeated impacts with a sinusoidally vibrating table", *Journal of Sound and Vibration*, **84**(2), pp. 173-189.

[41] Pustylinikov, L. D., 1977, "Stable and oscillating motions in nonautonomous dynamical systems", *Transactions of the Moscow Mathematical Society*, **34**(2), pp. 1-101.

[42] Wood, L. A., and Byrne, K. P., 1982, "Experimental investigation of a random repeated impact process", *Journal of Sound and Vibration*, **85**(1), pp. 53-69.

[43] Luo, A. C. J., and Han, R. P. S., 1996, "The dynamics of a bouncing ball with a sinusoidally vibrating table revisited", *Nonlinear Dynamics*, **10**, pp. 1-18.

[44] Bapat, C. N., and Sankar, S., 1986, "Repeated impacts on a sinusoidally vibrating table reappraised", *Journal of Sound and Vibration*, **108**(1),pp. 99-115.

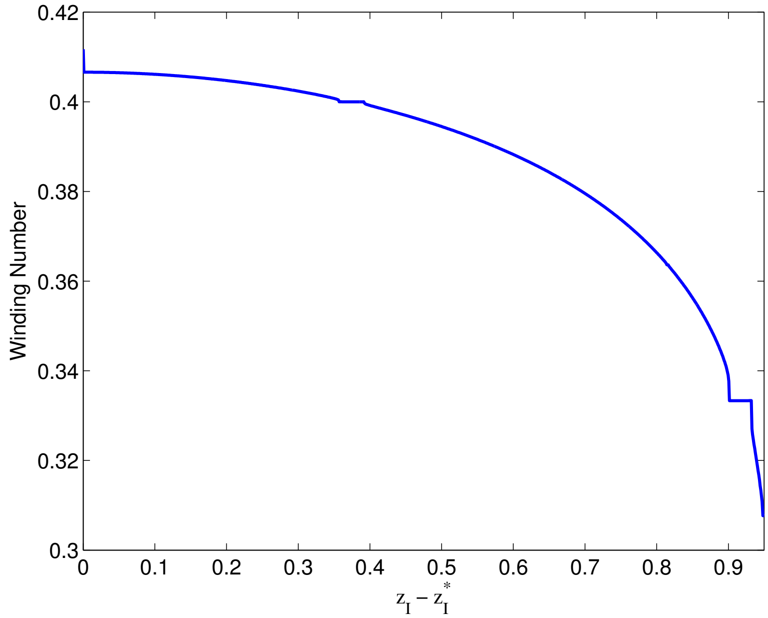

Figure 12: Winding number vs. $z_I - z_I^*$ for the quasiperiodic solutions of Eq. (1) around the period-one solution corresponding to $z_I^* = -\pi/2$ and $\phi_I^* = -\pi/3$ for $A = 1$ and $\omega = 1$.

[45] Tufillaro, N., B., Abbott, T., and Reilly, J., P., 1992, *An Experimental Approach to Nonlinear Dynamics and Chaos*, Addison-Wesley, New York, USA.

[46] Chirikov, B. V., 1979, "A universal instability of many dimensional oscillator systems", *Physics Reports*, **52**(5), pp. 263-379.

[47] Greene, J. M., 1980, "A method for determining a stochastic transition", *Journal of Mathematical Physics*, **20**(6), pp. 1183-1201.

[48] Lichtenberg, A. J., and Lieberman, M. A., 1992, *Regular and Chaotic Dynamics*, Springer-Verlag, New York, USA.

[49] http://www.lord.com/Home/MagnetoRheologicalMRFluid/Applications/PrimarySuspension/tabid/3329/Default.aspx

[50] Gelfreich, V. G., 2000, "Splitting of a small separatrix loop near the saddle-center bifurcation in area-preserving maps", *Physica D*, **136**, pp. 266-279.

[51] Diminnie, D. C., Haberman, R. 2002, "Slow passage through homoclinic orbits for the unfolding of a saddle-center bifurcation and the change in the adiabatic invariant", *Physica D*, **162**, pp. 34-52.

[52] Dankowicz, H. and Zhao, X., 2005. "Local analysis of co-dimension-one and co-dimension-two grazing bifurcations in impact microactuators", *Physica D*, **202**, (3-4), pp. 238-257.

[53] Kowalczyk, P., di Bernardo, M., Champneys, A. R., Hogan, S. J., Piiroinen, P. T., Kuznetsov, Yu. A., and Nordmark, A., 2006. "Two-parameter discontinuity-induced bifurcations of limit cycles: classification and open problems", *International Journal of Bifurcation and Chaos*, **16**(3), pp. 601-629.

[54] Abarbanel, H. D. I., 1996. *Analysis of observed chaotic data*, Springer, New York, USA.

[55] Smale, S., 1967. "Differentiable dynamical systems", *Bulletins of the American Mathematical Society*, **73**, pp. 747-817.

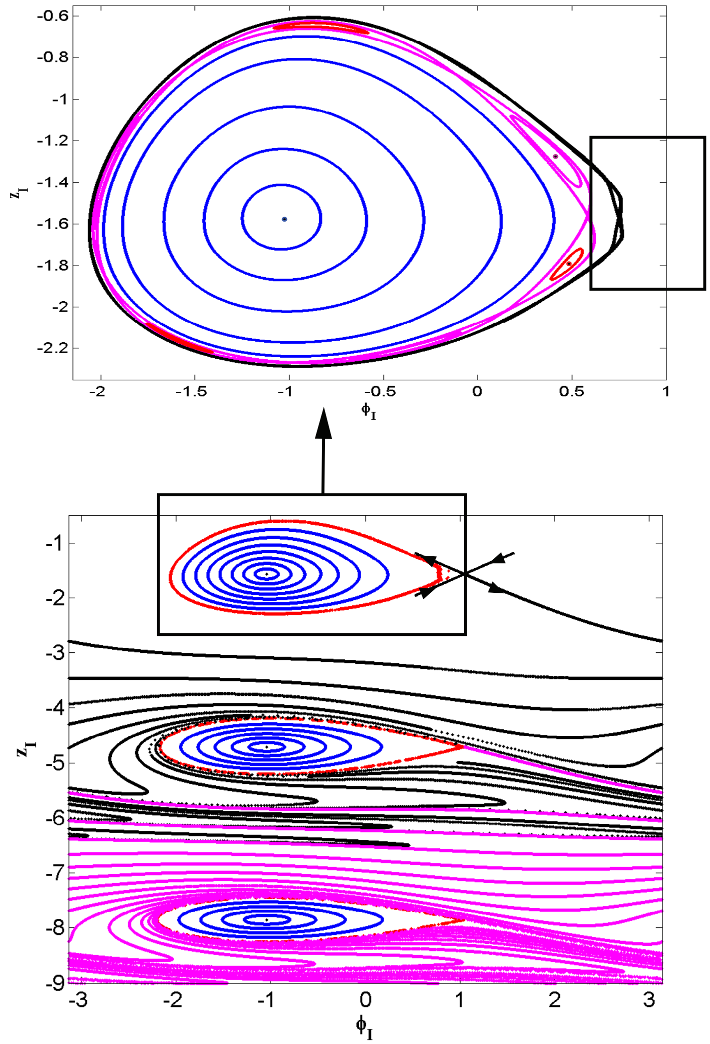

Figure 13: Dynamics around first three centers and saddles in ϕ_I-z_I plane for $A = 1$ and $\omega = 1$.

A Numerical algorithm to obtain the first positive root of a second order polynomial containing a cosine term

The first positive root of Eqs. (26) and (29) can be obtained by forward marching in time with a suitably chosen time step as in [45]. To obtain the first root with sufficient numerical accuracy, the time step required might be very small when there are two roots close to each other which renders the time-marching algorithm inefficient. This motivates the development of an algorithm wherein we identify disjoint intervals which can contain only a single root and use standard numerical root-finding algorithms like the bisection method in these intervals to locate the roots therein.

The switching conditions, Eqs. (26) and (29), can be written in the general form as

$$a\,t^2 + b\,t + c - d\cos(\omega\,t + \phi) \;=\; 0\,. \tag{77}$$

First we reduce the number of free parameters in Eq. (77) by dividing throughout by d and scaling time as $\tau = \omega\,t$. This reduces Eq. (77) to

$$a_1\,\tau^2 + b_1\,\tau + c_1 - \cos(\tau + \phi) \;=\; 0\,, \tag{78}$$

where $a_1 = \dfrac{a}{d\,\omega^2}$, $b_1 = \dfrac{b}{d\,\omega}$ and $c_1 = \dfrac{c}{d}$. The first root t of Eq. (77) is related to the first root τ of Eq. (78) as $t = \dfrac{\tau}{\omega}$. The algorithm for reliably obtaining the first root of Eq. (78) can be summarized as follows:

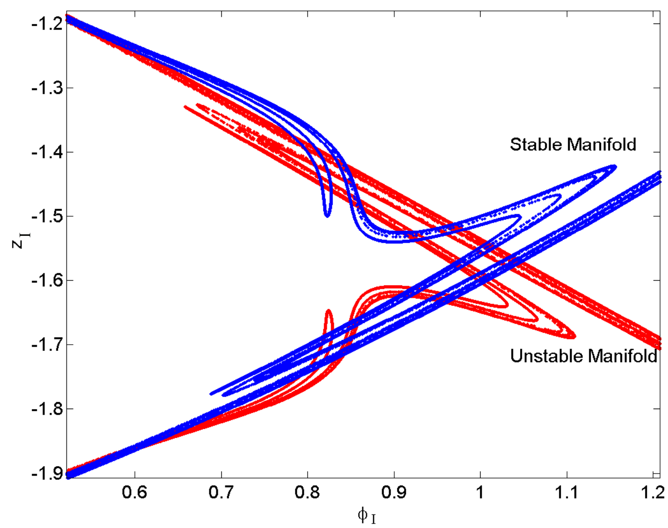

Figure 14: Dynamics in ϕ_I-z_I plane for $A = 1$ and $\omega = 1$ showing transverse intersection of the stable and unstable manifolds of the saddle. The region corresponds to the boxed region in Fig. 13 (top).

1. The first step involves identifying the intervals in which the roots of Eq. (78) can possibly exist. To determine these intervals, Eq. (78) is rewritten as $f(\tau) - g(\tau) = 0$ where $f(\tau) = a_1\,\tau^2 + b_1\,\tau + c_1$ and $g(\tau) = \cos(\tau + \phi)$. Since $|g(\tau)| \leq 1$, feasible intervals for the roots of $f(\tau) - g(\tau) = 0$ are determined by the roots of $f(\tau) \pm 1 = 0$. We define the set of real positive roots of $f(\tau) \pm 1 = 0$ as $R = \{r_i \in \mathbb{R}^+ | f(r_i) \pm 1 = 0\}$. The feasible intervals are now determined by the cardinality of the set R (denoted by $n(R)$) along with the members of R as follows. For $n(R) = 0$, there are no real positive roots of $f(\tau) - g(\tau) = 0$. For $n(R) > 0$, the feasible intervals for the roots are given by $[0, r_1]$ for $n(R) = 1$, $[r_1, r_2]$ for $n(R) = 2$, $[0, r_1] \bigcup [r_2, r_3]$ for $n(R) = 3$ and $[r_1, r_2] \bigcup [r_3, r_4]$ for $n = 4$, where $0 < r_1 < r_2 < r_3 < r_4$.

2. Each of the feasible intervals for the roots of $f(\tau) - g(\tau) = 0$ determined in the previous step can have multiple number of roots. The next step in the algorithm, therefore, involves partitioning the above intervals into sub-intervals (not necessarily of equal length) such that each sub-interval can have exactly one root. But this can only happen if the function is monotonic in that sub-interval. To ensure this, we use the fact that a function is monotonic in the interval in which its derivative has the same sign and hence, can have only one root in that interval. This requirement can be met if somehow we can guarantee that our 'target sub-interval' (which we seek to obtain in a way that it contains either zero or exactly one root) contains exactly one inflexion point of the slopes.

   Thus, we simply need to compute the zeros of the second derivative of the function and then construct the sub-intervals such that each sub-interval contains exactly one zero of the second derivative, hence exactly one inflexion point of the first derivative and hence the monotonicity, of the function itself, is guaranteed. As a result, now the bisection algorithm can be applied as we already know that the sub-interval on which we are applying bisection, contains at most one root. To perform the above partition, we proceed as follows:

   (a) Since $f''(\tau) = 2\,a_1$ and $g''(\tau) = -\cos(\tau + \phi)$, the roots of $f''(\tau) - g''(\tau) = 0$ can be obtained in closed form (for $|a_1| \leq \dfrac{1}{2}$) as

   $$\tau_{dd} = 2\,m\,\pi \pm (\arccos(-2\,a_1) - \phi)\ , \quad m = 0, 1, 2, \cdots .$$

   For $|a_1| > \dfrac{1}{2}$, $f''(\tau) - g''(\tau) = 0$ has no real roots. The roots τ_{dd} along with the endpoints of the feasible intervals provide a partition of the feasible intervals into feasible sub-intervals such that $f'(\tau) - g'(\tau) = 0$ can have only one root in each subinterval. It can be noted that all numerical simulations given in this paper accord with the condition $|a_1| \leq \dfrac{1}{2}$, namely forcing amplitude is chosen in a way such that it does not exceed unity.

(b) The existence of roots of $f'(\tau) - g'(\tau) = 0$ in the sub-intervals determined in the previous step is ascertained by evaluating $f'(\tau) - g'(\tau)$ at the endpoints of the subinterval. If the value is zero at either of the end-points, that end-point is the root τ_d of $f'(\tau) - g'(\tau) = 0$. If the function $f'(\tau) - g'(\tau)$ changes sign at the end-points, there is a root τ_d in the subinterval which can be obtained using the bisection method otherwise there is no root in that sub-interval. The roots τ_d of $f'(\tau) - g'(\tau) = 0$ in each of the subintervals along with the end-points of the feasible intervals form a partition of the feasible intervals into sub-intervals such that $f(\tau) - g(\tau) = 0$ can have only one root in each subinterval.

3. Having obtained sub-intervals of the semi-real axis $\mathbb{R}^+$ such that there can be exactly one root of the function $f(\tau) - g(\tau) = 0$ in each sub-interval, each sub-interval is checked for the roots analogous to the procedure described for the roots of $f'(\tau) - g'(\tau)$ in the previous step. The procedure starts with the first sub-interval and is terminated if either a root is obtained or all the sub-intervals are exhausted in which case there are no real positive roots of Eq. (78).

B Grazing discontinuities in the switching times

As mentioned in Appendix A, determination of the switching times require solution of Eqs. (26) and (29) which are of the form of Eq. (77). Geometrically, the roots of the transcendental equation (77) represent points of intersection of a parabola and a cosine curve. Since the parameters b, c and ϕ in the above equation depend on the state variables z_I and ϕ_I, or z_{II} and ϕ_{II}, therefore, the switching times t_I and t_{II} are functions of the state variables z_I and ϕ_I, and z_{II} and ϕ_{II}, respectively. A 3D plot of this function for the first switching time $t_I(z_I, \phi_I)$ for $A = 1$ and $\omega = 1$, and $z_I \in [-4, 0]$ and $\phi_I \in [-\pi, \pi]$ is shown in Fig. 15.

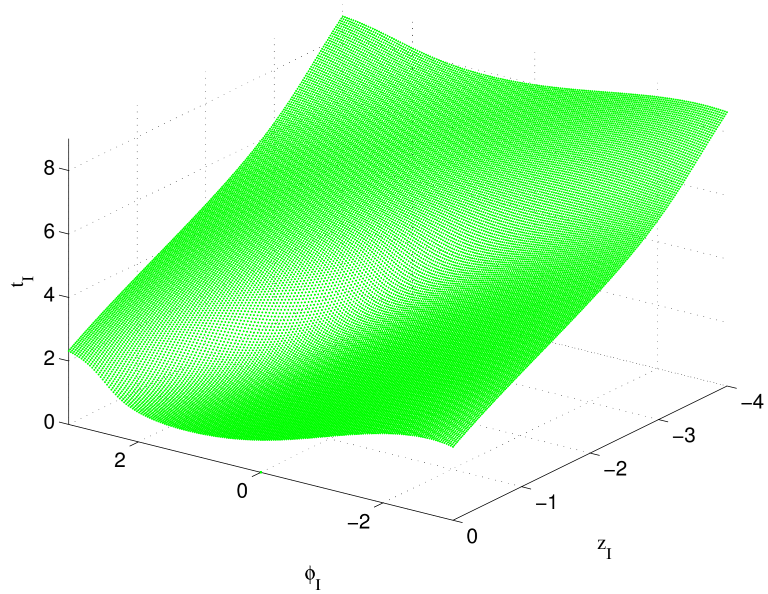

Figure 15: A 3D plot of the function $t_I(z_I, \phi_I)$ for $A = 1$ and $\omega = 1$.

From Fig. 15, we note that the function defines a smooth surface for these parameter values. However, the function for the switching times can in general have discontinuities corresponding to a grazing intersection of the parabola and the trigonometric function as shown in Fig. 16. The first intersection of the parabola and the trigonometric function is shown by a $*$. It can be seen from Fig. 16 that a small change in the parameters result in a large discontinuous change in the first intersection point.

For a grazing intersection, the velocity at the instant of switching t_I is zero as well. Hence, the equations related to the grazing intersection are given by

$$\frac{1}{2}t_I^2 + z_I t_I + \frac{A}{\omega^2}\cos(\phi_I) - \frac{A}{\omega^2}\cos(\omega t_I + \phi_I) - 1 = 0$$

and

$$t_I + z_I + \frac{A}{\omega}\sin(\omega t_I + \phi_I) = 0\,.$$

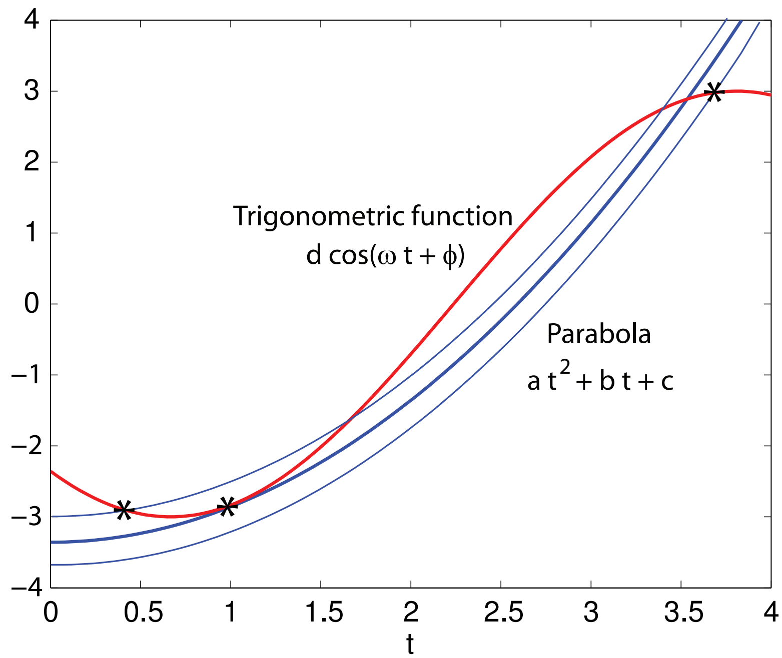

Figure 16: Grazing intersection of a parabola and the cosine curve.

For a given set of parameters A and ω, a point in the plane (z_I, ϕ_I) for which the above set of equations is satisfied for some real positive t_I is a grazing point. We define the set of all grazing points in the plane (z_I, ϕ_I) as the grazing curve for that particular set of parameters A and ω. From the above set of equations, the switching time t_I can be solved in closed form in terms of z_I, ϕ_I, A and ω using trigonometric elimination. However, our aim is to get the grazing curves and not necessarily the switching time at grazing. We use a fixed arc-length based continuation scheme (see [?]) in conjunction with the Newton-Raphson method to obtain these grazing curves. The grazing curves for $A = 3$ and different values of ω are plotted in Fig. 17. Thick lines represent the curves of actual discontinuities in t_I and thin dotted lines represent the case when the grazing root is the second root and hence does not correspond to a discontinuity in t_I. These two curves form a closed loop in the $z_I - \phi_I$ plane. A 3D plot of the function $t_I(z_I, \phi_I)$ for $A = 3$ and $\omega = 1$ is shown in Fig. 18 which clearly illustrates the discontinuities in the function $t_(z_I, \phi_I)$. Also plotted with a thick line is the grazing curve. It can be seen that the discontinuities in the function $t_I(z_I, \phi_I)$ correspond exactly to the grazing curve.

It can be seen from Fig. 17 that the length of the grazing curves decrease with increasing ω. In general, there exist a value of $\omega = \omega_{\text{critical}}$ for which this loop degenerates into a point. For $\omega > \omega_{\text{critical}}$, there are no discontinuities in the function $t_I(z_I, \phi_I)$. This value of ω_{critical} decreases with a decrease in the other parameter A. It has been observed numerically that $\omega_{\text{critical}} \to 0$ as $A \to 1$ from above. This implies that for $A \le 1$, there are no discontinuities in the function $t_I(z_I, \phi_I)$ for any ω. This can be demonstrated as follows:

The acceleration of the subsystem I is given by

$$\ddot{x}_I(t) = 1 + A\cos(\omega t + \phi)\,.$$

For $A \le 1$, $\ddot{x}_I(t) \ge 0$ and hence the velocity of the subsystem is monotonic and non-decreasing. Therefore, the equation $\dot{x}_I(t) = 0$ can have only one real root. Next, we consider two cases: $\dot{x}_I(0) \ge 0$ and $\dot{x}_I(0) < 0$.

1. For the case of $\dot{x}_I(0) \ge 0$, $\dot{x}_I(t) > 0$ for $t > 0$. Therefore, $\dot{x}_I(t_I) > 0$ where t_I is the root of $x_I(t_I) - 1 = 0$. Hence, the two equations $x_I(t) - 1 = 0$ and $\dot{x}_I(t) = 0$ cannot hold simultaneously. This implies that there can be no grazing intersection and accordingly no discontinuities in the function $t_I(z_I, \phi_I)$ for any value of ω.

2. For the case of $\dot{x}_I(0) < 0$, the equation $x_I(t) = 0$ has a single root say $t = t_d$. However, for $t \in [0, t_d)$, $\dot{x}(t) < 0$ and therefore, the displacement $x(t)$ is monotonically decreasing in this interval. Since $x(0) = 0$, it follows that $x(t_d) < 0$ and therefore, $x(t_d) - 1 < 0$. Again this implies that the two equations $x_I(t) - 1 = 0$ and $\dot{x}_I(t) = 0$ cannot hold simultaneously and hence, there can be no discontinuities in the function $t_I(z_I, \phi_I)$.

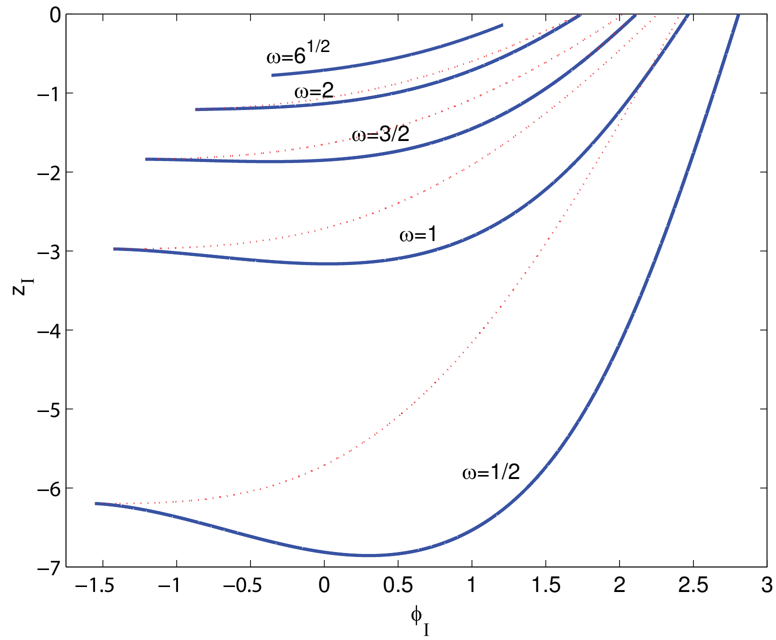

Figure 17: Grazing curves for $A = 3$. Thick lines represent the curves of actual discontinuities in t_I and thin dotted lines represent the case when the grazing root is the second root and hence does not correspond to a discontinuity in t_I.

Hence, for $A \leq 1$, the function $t_I(z_I, \phi_I)$ is continuous for any value of the parameter ω.

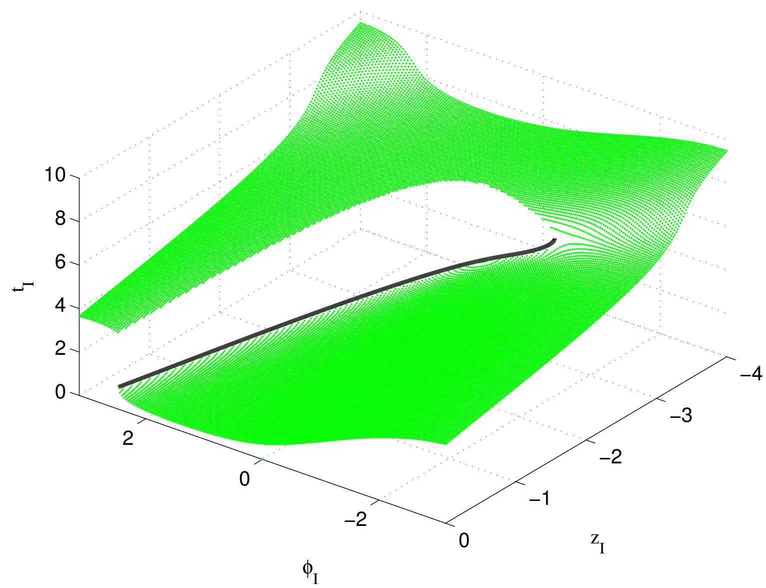

Figure 18: A 3D plot of the function $t_I(z_I, \phi_I)$ for $A = 3$ and $\omega = 1$.